

A universal reagent for detection of emerging diseases using bioengineered multifunctional yeast nanofragments

Received: 30 December 2021

Accepted: 4 May 2023

Published online: 8 June 2023

 Check for updates

Junrong Li¹, Christopher B. Howard¹, Shuvashis Dey¹, Kym Lowry^{2,3}, David M. Whiley², Simon Puttick⁴, Stephen Rose⁴, Richard J. Lobb¹, Alain Wuethrich¹ & Selvakumar Edwardraja¹ & Matt Trau^{1,5}

Accurate and early detection of biomarkers provides the molecular evidence for disease management, allowing prompt actions and timely treatments to save lives. Multivalent biomolecular interactions between the probe and biomarker as well as controlled probe orientation on material surfaces are keys for highly sensitive detection. Here we report the bioengineering of programmable and multifunctional nanoprobe, which can provide rapid, specific and highly sensitive detection of emerging diseases in a range of widely used diagnostic systems. These nanoprobe composed of nanosized cell wall fragments, termed as synthetic bionanofragments (SynBioNFs), are generated by the fragmentation of genetically programmed yeast cells. SynBioNFs display multiple copies of biomolecules for high-affinity target binding and molecular handles for the precisely orientated attachment on surfaces used in diagnostic platforms. SynBioNFs are demonstrated for the capture and detection of SARS-CoV-2 virions using multiple diagnostic platforms, including surface-enhanced Raman scattering, fluorescence, electrochemical and colorimetric-based lateral flow systems with sensitivity comparable with the gold-standard reverse-transcription quantitative polymerase chain reaction.

Biomarkers, defined as measurable indicators of disease, are valuable tools for patient screening, prognosis, informing treatment and treatment monitoring. The detection of biomarkers typically relies on functional nanoprobe (for example, labelled antibody or peptide) due to their high sensitivity and specificity¹. Ideal functional nanoprobe should have high binding affinity to the target, cost-effective production, scalability and flexible storage to benefit population-based patient screening, which is particularly important for the rapid detection of

emerging diseases like COVID-19 (refs. 2,3). The controlled and precise attachment of the target binder (for example, antibody) to material surfaces in optimal densities and orientations to maximize the binding affinity, multivalency and target-specific recognition are also crucial for improved diagnostic outcomes⁴⁻⁶. Although various strategies are available for attaching biomolecules to materials, these methods are challenging because of problems with conjugation efficiency, site specificity and inhibited target binding. As such, it is important to

¹Centre for Personalised Nanomedicine, Australian Institute for Bioengineering and Nanotechnology (AIBN), The University of Queensland, Brisbane, Queensland, Australia. ²Centre for Clinical Research, Faculty of Medicine, The University of Queensland, Royal Brisbane and Women's Hospital, Brisbane, Queensland, Australia. ³Queensland Paediatric Infectious Diseases (QPID) Sakzewski Laboratory, Queensland Children's Hospital, Brisbane, Queensland, Australia. ⁴Probing Biosystems Future Science Platform, Commonwealth Scientific and Industrial Research Organization, Brisbane, Queensland, Australia. ⁵School of Chemistry and Molecular Biosciences, The University of Queensland, Brisbane, Queensland, Australia. ✉e-mail: c.howard2@uq.edu.au; a.wuethrich@uq.edu.au; s.edwardraja@uq.edu.au; m.trau@uq.edu.au

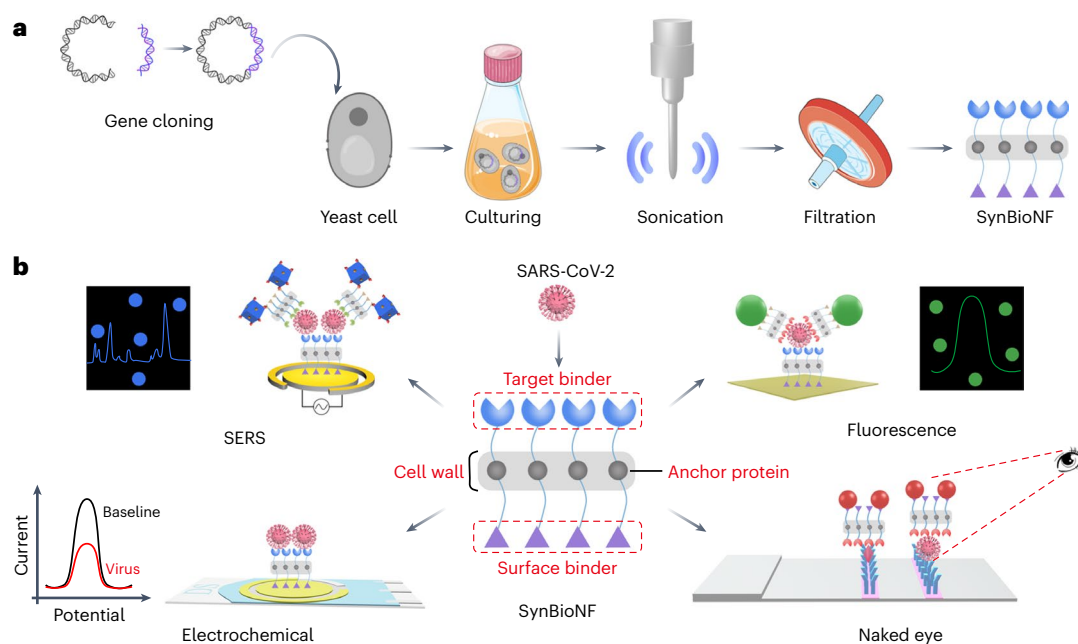


Fig. 1 | Design of SynBioNFs as a reagent for disease detection. a, b, Generation (a) and universal application (b) of SynBioNFs in the detection of SCV2 on diagnostic platforms including SERS, fluorescence, electrochemical and naked-eye lateral flow platforms. The following capture and/or detection SynBioNFs pairings were used: capture SynBioNFs (W25–MatterTag) and detection SynBioNFs (Sb68–SpyTag) on the SERS platform; capture SynBioNFs

(Sb68–MatterTag) and detection SynBioNFs (Nb21–StrepTag) on the fluorescent platform; capture SynBioNFs (Sb68–MatterTag) on gold electrodes for electrochemical detection; and SynBioNFs (Nb21–SpyTag) conjugated with SpyCatcher-coated spherical gold particles used as the detection reagents for LFA.

develop better approaches to overcome such challenges for effective disease detection.

Here we developed a class of bioinspired multifunctional nanoprobes based on yeast-cell-derived synthetic bionanofragments (SynBioNFs) for the rapid detection of emerging diseases. SynBioNFs were genetically programmed to display multifunctional components including specific target binder (nanobody) and generic surface binder (adhesive peptide) anchored on nanosized yeast cell wall fragments through the endogenous yeast cell wall protein Aga2p. We demonstrated the universal nature of SynBioNFs through their utility in SARS-CoV-2 (SCV2) virion detection on various detection platforms, including surface-enhanced Raman scattering (SERS), fluorescence, electrochemical and colorimetric lateral flow assay (LFA) systems.

SynBioNFs as multifunctional nanoprobes

To allow highly efficient and effective biomarker detection, we genetically engineered SynBioNFs to express multifunctional protein or peptide components on the cell wall via a yeast surface display system, followed by simple fragmentation and separation of cell wall fragments into nanosized particles (Fig. 1a). As a proof-of-concept demonstration of their use in disease detection, SynBioNFs displaying anti-SCV2 receptor-binding-domain (RBD) nanobodies (W25 (ref. 7), Sb68 (ref. 8) and Nb21 (ref. 6)) were applied on different diagnostic platforms for the detection of SCV2 (Fig. 1b), including SERS, fluorescence, electrochemical and LFA systems. Nanobodies, the smallest antigen-binding domain, were selected as the recognition module due to their high binding affinity, stability and suitability for large-scale production^{9,10}. MatterTags¹¹, SpyTags^{4,9} and StrepTags¹² were used for the tethering of SynBioNFs to various surfaces used in the diagnostic platforms. Specifically, MatterTag—a type of adhesion-promoting peptide—is able to attach to various surfaces (for example, gold, silicon and plastic) via both hydrophobic and polar interactions¹¹. SpyTag enables a spontaneous covalent conjugation with SpyCatcher for surface immobilization,

which is a rapid self-catalysed assembly process^{4,9}. StrepTag allows the specific interaction with streptavidin for an easy surface coupling with commercially available streptavidin-functionalized particles. The use of a defined biological immobilization strategy instead of non-specific chemistry approach preserved the binding function as well as ensured the precisely controlled orientation of the nanobody.

Compared with commercially available antibodies in biomarker detection, SynBioNFs featured a higher stability under the conditions of high temperature (Supplementary Fig. 1), low pH and strong detergents (Supplementary Fig. 2a–c), as well as sufficient stability in the presence of high concentrations of salt (Supplementary Fig. 2d), which largely resulted from the stabilization of functional proteins by the abundant hydroxyl groups of polysaccharides in the yeast cell wall^{13,14}. Furthermore, SynBioNFs demonstrated higher avidity towards targets due to the capability of loading multiple copies of functional proteins by the nanosized yeast cell wall fragments (Supplementary Fig. 3). Additionally, SynBioNFs demonstrated a much weaker disassociation than the corresponding nanobody (Supplementary Fig. 4). Thus, SynBioNFs with high stability and high avidity can undoubtedly benefit the widespread and highly sensitive biomarker detection, especially for pandemic disease screening.

Generation and characterization of SynBioNFs

We employed yeast surface display to project the desired nanobodies on the cell wall due to several advantages, including cost-effective growth media, robustness in the fermentor and availability of well-established genetic tools to precisely edit the yeast cell¹⁵. A panel of nanobodies targeting distinct epitopes of SCV2 RBD (W25, Sb68 and Nb21) were bioengineered on the N terminal of the yeast surface protein Aga2p, connected via a 15 amino acid flexible GGGGS linker. To enable the attachment of SynBioNFs to material surfaces, surface-binding peptides including either MatterTag, SpyTag or StrepTag were added to the C terminus of the Aga2p protein through a 30 amino acid flexible GGGGS linker. The flexible GGGGS linkers added on either side of the

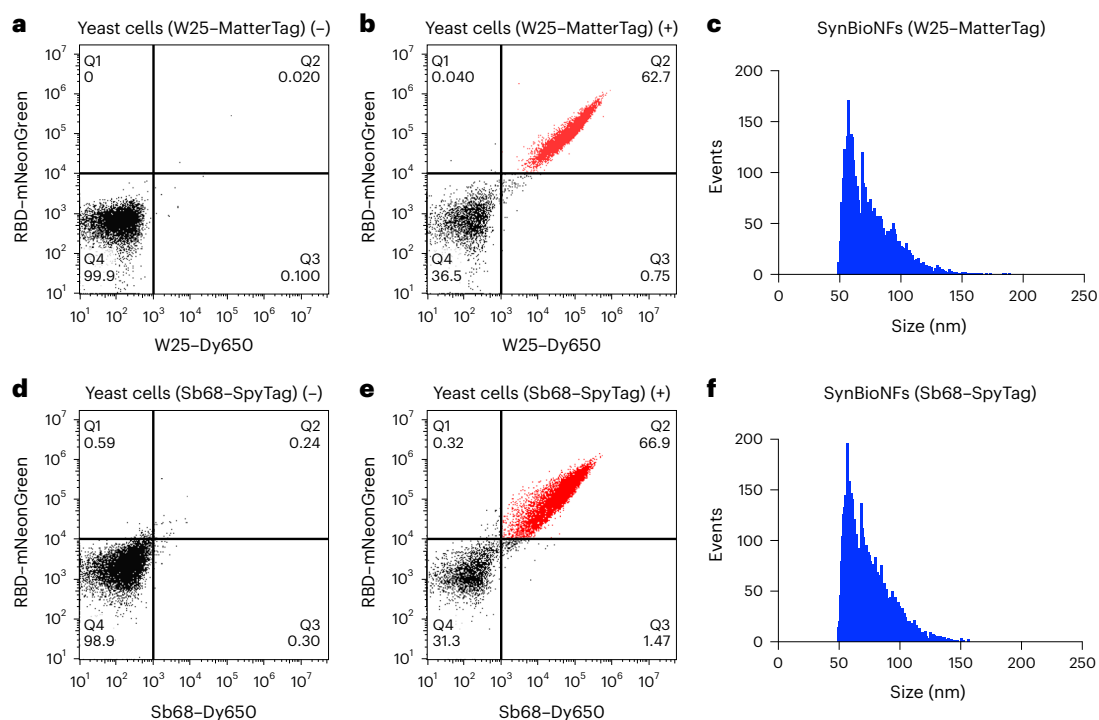


Fig. 2 | Profiling of fusion protein expression on yeast cell surfaces and size characterization of the corresponding SynBioNFs. a, b, d, e. Flow cytometry analysis of yeast cell (a and d) controls and positives with W25–MatterTag (b)

and Sb68–SpyTag (e) expressions. c, f. Nanoflow cytometry measurement of the particle size distribution of SynBioNFs (W25–MatterTag) (c) and SynBioNFs (Sb68–SpyTag) (f).

Aga2p anchor protein were used to minimize steric hindrances between the nanobody and functional peptide fusions. Haemagglutinin (HA) and c-Myc epitope tags were also engineered at the N and C termini to allow the detection of the displayed fusion proteins.

Flow cytometry was utilized to determine nanobody display on the yeast cell surface and nanobody binding to the SCV2 RBD protein. Specifically, yeast cells induced to display nanobodies were labelled with the fluorescent anti-myc-Dy650 antibody to detect nanobody cell surface expression. The cells were also labelled with fluorescent SCV2 RBD–mNeonGreen to determine the nanobody-binding affinity towards SCV2 RBD. As two representative examples, yeast cells encoding W25–MatterTag and Sb68–SpyTag showed the expression of nanobodies on over 60% of yeast cells (Fig. 2a,b,d,e), suggesting a high level of protein expression in the commonly employed plasmid-based approach^{16–19}. Furthermore, the Sb68–SpyTag fusion protein on the yeast cells revealed a binding affinity to the SCV2 RBD ($k_D = 42$ nM) similar to the soluble Sb68 nanobody ($k_D = 37$ nM)⁸ (Supplementary Fig. 5), confirming that the fusion design and surface display retained the complete function of the nanobody.

SynBioNFs carrying W25–MatterTag and Sb68–SpyTag were generated through mechanically fragmenting the yeast cells via sonication that had no detrimental effect on the protein activity (Supplementary Fig. 6). Using the filters with 100 nm cut-off to further purify the products, the obtained SynBioNFs possessed a mode size of approximately 70 nm as measured by nanoflow cytometry (Fig. 2c,f).

SynBioNFs as capture nanoprobes

Gold surfaces provide a common interface to accommodate capture probes in biomarker detection²⁰. We demonstrated SynBioNF functionalization on gold surfaces in one-step incubation using MatterTag-assisted immobilization, which allows a biological functionalization on gold surfaces for site-specific anchoring, and potentially enhancing SynBioNF orientation on the surface for optimal target recognition.

We immobilized SynBioNFs (W25–MatterTag) on gold microelectrode surfaces to act as capture nanoprobes (Fig. 3a). Before the immobilization, we utilized oxygen plasma cleaning on the gold microelectrodes to remove potential contamination²¹, which produced a similar performance to traditional electrochemical cleaning^{22,23}, as demonstrated by differential pulse voltammetry (DPV) and cyclic voltammetry (CV) results (Supplementary Fig. 7). To confirm the MatterTag-assisted immobilization of SynBioNFs, we monitored the redox reaction of $[\text{Fe}(\text{CN})_6]^{3-/4-}$ on gold microelectrodes through Faradaic electrochemical impedance spectroscopy, DPV and CV. As shown by the Nyquist plot, an increase in the surface impedance is observed following the addition of SynBioNFs on the gold microelectrodes due to the attenuated electron transfer (Fig. 3b). In agreement with electrochemical impedance spectroscopy, DPV also demonstrated a substantial reduction in peak current following the incubation of gold surface with SynBioNFs (Fig. 3c). Furthermore, the corresponding CV data indicated the characteristic redox peak of our electrochemical biosensors (Fig. 3d). Additionally, we evaluated the role of MatterTag in assisting the binding of capture SynBioNFs on gold microelectrodes using our SERS platform, which indicated an enhanced capture of the SCV2 RBD target through MatterTag for a higher SERS signal output (Fig. 3e,f). The SERS signal resulting from the identification of SCV2 RBD by detection SynBioNFs conjugated to plasmonic SERS nanoboxes is explained in the following sections.

We also determined the required time of MatterTag-assisted SynBioNF immobilization on gold surfaces by measuring the percentage peak current changes in the DPV responses. Supplementary Fig. 8 reveals the complete binding of SynBioNFs on gold surfaces within a 10 min reaction, which was in line with the MatterTag-assisted soluble protein immobilization on material surfaces¹¹.

SynBioNFs as detection nanoprobes

The conjugation of SynBioNFs with plasmonic nanostructures generated detection nanoprobes for reading highly specific and sensitive

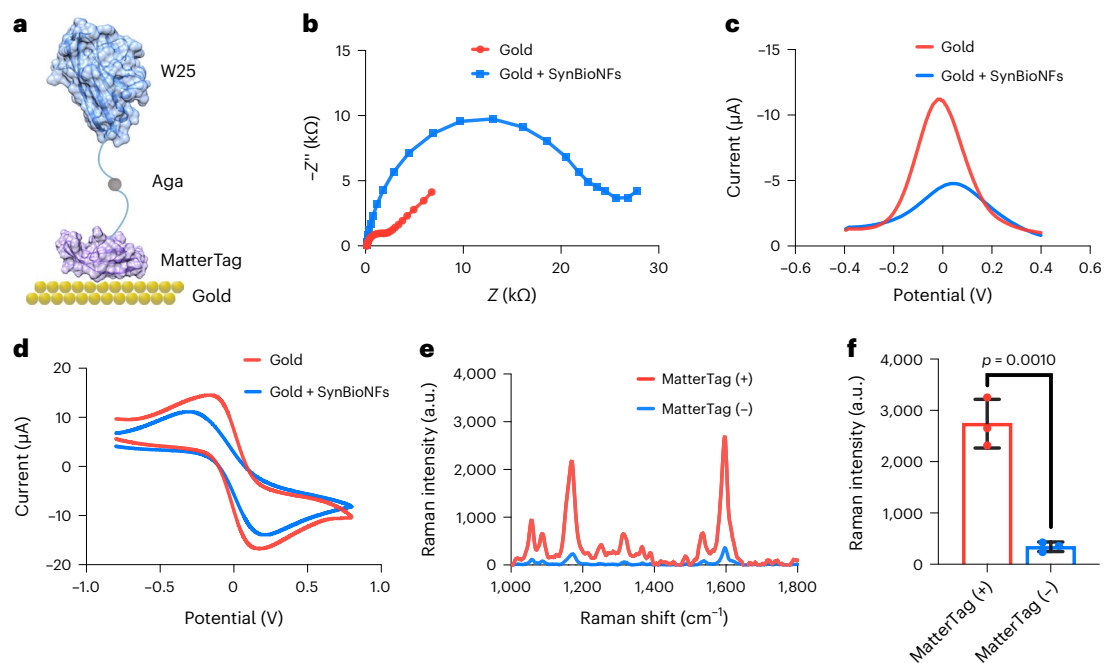


Fig. 3 | Evaluation of MatterTag-assisted SynBioNF immobilization on gold microelectrodes. **a**, Schematic of the attachment of SynBioNFs to gold via MatterTag. **b–d**, Electrochemical study of gold microelectrode versus gold microelectrode with SynBioNFs (W25–MatterTag), showing the Nyquist plots (**b**), DPV responses (**c**) and CV characterization (**d**). **e, f**, SERS result of the

representative Raman spectra (**e**) and Raman intensities (**f**) at $1,603\text{ cm}^{-1}$ of SCV2 RBD detection by coating gold microelectrodes using SynBioNFs infused with MatterTag (red) or without MatterTag (blue) ($p = 0.0010$, two-tailed t -test). Data are presented as mean values \pm standard deviation from three independent experiments.

signals. Anisotropic gold–silver alloy nanoboxes with strong Raman enhancement capability were selected as representative nanostructures to conjugate with SynBioNFs. Exploiting the SpyTag and SpyCatcher systems, SynBioNFs (Sb68–SpyTag) were incubated with SpyCatcher-coated nanoboxes for a simple self-assembly (Fig. 4a). After incubation with SynBioNFs, the nanoboxes with an average edge length of around 80 nm (Fig. 4b) were surrounded by a layer of low-contrast material (Supplementary Fig. 9), which indicated the conjugation of SynBioNFs on nanobox surfaces. Crucially, the use of SpyTag and SpyCatcher as a simple and modular approach for bioconjugation provided a potentially universal and useful strategy for biofunctionalization.

To demonstrate the crucial role of SpyTag and SpyCatcher in building the bioconjugates, we prepared different bioconjugates and reacted with RBD–mNeonGreen for fluorescence-based nanoflow cytometry profiling. For bioconjugate 1 prepared in the presence of SynBioNFs (SpyTag–Sb68) and nanoboxes (coated with SpyCatcher), the fluorescence intensities were substantially higher than the corresponding control (Fig. 4c). In contrast, bioconjugates 2 and 3 using nanoboxes without SpyCatcher or SynBioNFs without SpyTag showed remarkably low fluorescence intensities like their controls. The mean fluorescence intensity further quantitatively showed much higher intensities for bioconjugate 1 that had both SpyTag and SpyCatcher present (Fig. 4d). Such a result clearly supported the necessity of the SpyTag and SpyCatcher systems in connecting detection SynBioNFs and nanoboxes. These data also illustrated that the binding components (that is, nanobody) on SynBioNFs were highly functional even after conjugation with nanoboxes.

As demonstrated in previous reports, the SpyTag and SpyCatcher systems allowed a prompt autocatalytic reaction under physiological conditions and rapidly formed a covalent isopeptide bond^{4,9}. In our study, sodium dodecyl sulfate–polyacrylamide gel electrophoresis indeed revealed the formation of a peptide bond in ~ 1 min (Supplementary Fig. 10) using the purified SpyTag and SpyCatcher soluble

proteins. Similarly, the preparation of bioconjugates of SynBioNFs (Sb68–SpyTag) and nanoboxes (coated with SpyCatcher) demonstrated rapid assembly within 10 min, as suggested by the nanoflow cytometry measurement (Supplementary Fig. 11).

SynBioNF-enabled SCV2 detection on SERS platform

Having engineered SynBioNFs that can act as capture and detection nanoprobes, we showcased their application on the SERS platform for SCV2 detection (Fig. 5a–e). First, capture SynBioNFs (W25–MatterTag) were applied on gold microelectrodes by using the W25 nanobody to capture SCV2 by binding the class-2 epitope site of RBD on the spike protein⁷. Subsequently, detection SynBioNFs (Sb68–SpyTag) conjugated with nanoboxes (coated with SpyCatcher and Raman reporters) were introduced to achieve virus identification and highly sensitive signal readout. Unlike the W25 nanobody, Sb68 nanobody recognizes a class-4 epitope region of RBD and has high affinity towards RBD on the spike protein ($k_D = 37\text{ nM}$)⁸. As the RBD amounts positively correlated with the viral loads, the SCV2 concentration can be inferred from the Raman reporter (that is, 2,7-mercapto-4-methylcoumarin (MMC)) intensity at $1,603\text{ cm}^{-1}$. To further intensify the Raman readout for a highly sensitive and specific SCV2 detection, we integrated an alternating-current electrohydrodynamic-induced nanoscopic fluid flow (that is, nanomixing)²⁴ to improve the molecular collision of the sample and detection SynBioNFs with the gold microelectrodes (Supplementary Fig. 12).

Highly accurate identification of targets among a variety of biomolecules, which may be present in the samples, is crucial for a reliable diagnosis²⁰. To demonstrate the specificity of the engineered SynBioNFs in SCV2 detection, we challenged the designed SERS platform by analysing a range of samples, including recombinant SCV2 RBD protein, gamma-irradiated SCV2 virions, phosphate-buffered saline (PBS), cell culture medium, SCV2 S2 protein, recombinant influenza HA antigen, recombinant dengue virus 2 NS1 antigen and recombinant SARS-CoV-1

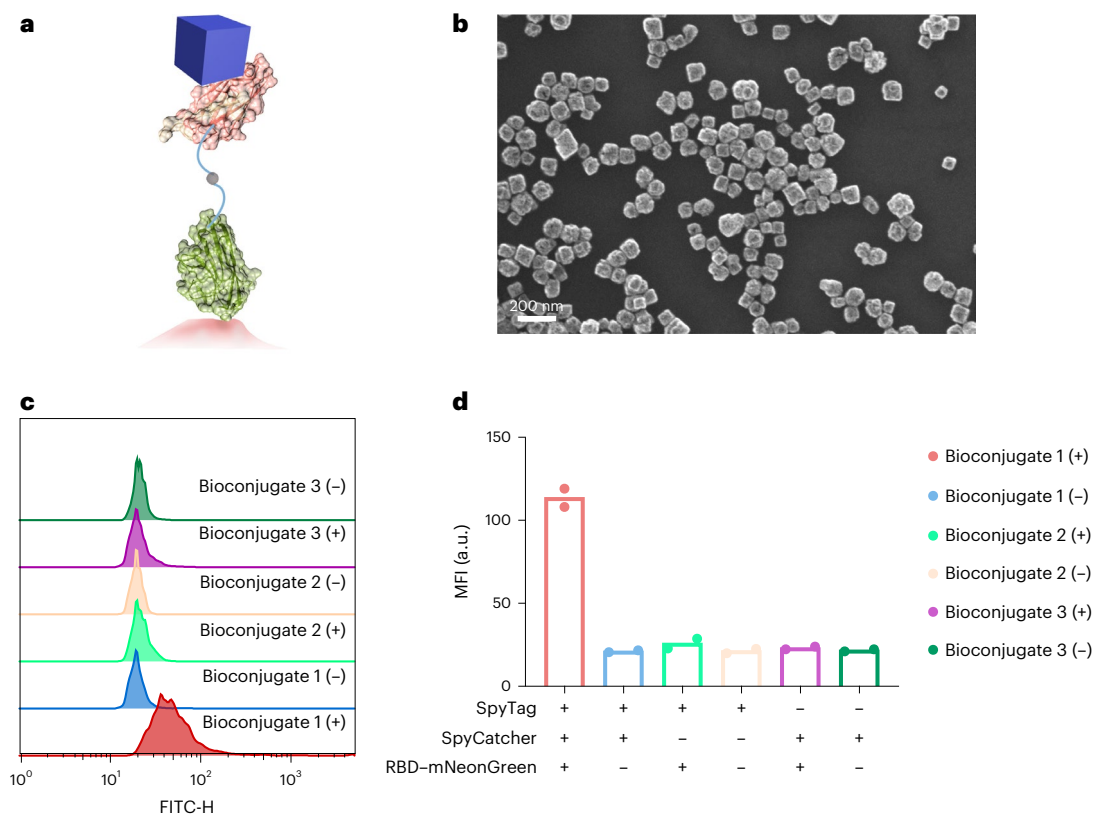


Fig. 4 | Demonstration of SpyTag and SpyCatcher systems in conjugating SynBioNFs with gold-silver alloy nanoboxes as detection nanoprobes. **a**, Schematic of SynBioNFs conjugated with nanoboxes for virus detection by identifying RBD on the spike protein. **b**, Scanning electron microscopy image of the nanoboxes, showing the successful preparation of nanoparticles with the desired box-like morphology. Data from one independent experiment. **c,d**, Histogram (**c**) and mean fluorescence intensities (MFIs) (**d**) of bioconjugates

measured in flow cytometry. Bioconjugates 1–3 were prepared with SynBioNFs (SpyTag–Sb68) and nanoboxes (coated with SpyCatcher), SynBioNFs (Sb68) and nanoboxes (coated with SpyCatcher) and SynBioNFs (SpyTag–Sb68) and nanoboxes, respectively, in which the (+) samples were reacted with RBD–mNeonGreen as positives and the (–) ones were incubated with PBS as controls. Data are presented as mean values from two independent experiments.

RBD protein. As shown in Fig. 5f,g, the positive samples displayed clear Raman signals due to the correct identification of the captured targets, whereas the negative controls showed negligible Raman signals without successful recognition. Therefore, this result illustrated the high specificity of SynBioNFs in reacting with RBD on SCV2.

The ability to detect a low concentration of SCV is critical for the timely control of disease spreading. We, therefore, examined the sensitivity of SynBioNF-enabled SCV2 detection by measuring the Raman signals from a titration of SCV2 gamma-irradiated virus culture (that is, 0, 10, 100, 1,000 and 10,000 virions μl^{-1}). In all the experiments, virus measurement refers to the number of copies of virus RNA to enable a comparison with reverse-transcription quantitative polymerase chain reaction (RT-qPCR)—the gold standard for SCV2 detection. As shown in Supplementary Fig. 13, an increase in the Raman signal was observed with the use of a higher viral concentration and consequently resulted in a good linear relationship curve ($R^2 = 0.99$) for quantification. The limit of detection of SCV2 detection was calculated to be 5.4 virions μl^{-1} based on three times the standard deviation of blank signals, which was comparable with the RT-qPCR result (~ 1 copies μl^{-1})²⁵ and avoided the potential bias arising from non-specific amplification events. In particular, the SynBioNF-enabled SERS platform allowed the differentiation of simulated patients and healthy controls by titrating a low concentration of gamma-irradiated SCV2 into human saliva (that is, 0, 10 and 100 virions μl^{-1}) (Supplementary Fig. 14), suggesting the potential use in clinical settings²⁶.

For clinical relevance, we utilized the SynBioNF-enabled SERS platform to screen a panel of 134 nasopharyngeal swab samples

from patients (84 SCV2 positives and 50 negatives, as confirmed by RT-qPCR). The representative Raman images and the acquired Raman intensities at $1,603\text{ cm}^{-1}$ of all the clinical samples clearly showed identifiable signals for positive samples but negligible signals for negative ones (Fig. 6a,b). Based on the cut-off value of 94 to classify patients and correlate with RT-qPCR diagnosis, SynBioNFs enabled the identification of 81 positives and 50 negatives (Fig. 6c), which correspond to the sensitivity, specificity and accuracy of 96.43%, 100.00% and 97.76%, respectively. Furthermore, this detection achieved a good receiver operating characteristic graph with an area under the curve of 0.9984 (Fig. 6d). Comparing the normalized Raman intensities with cycle threshold (Ct) values of positive samples, a Bland–Altman analysis suggested no significant difference between SynBioNF-enabled and RT-qPCR detections as the majority of the data fit in the 95% limits of agreement (Fig. 6e). In a selected number of samples near the limit of detection of the SynBioNF-enabled SERS platform, we noticed a variation in Raman intensities of positive samples with RT-qPCR tests (Supplementary Fig. 15), which was probably caused by the different working principles of these two approaches and was also reported in a previous finding⁹. Additionally, SynBioNFs enabled the detection of different SCV2 variants (that is, Delta and Omicron) (Fig. 6f), which was beneficial for accurate SCV2 screening.

Furthermore, we compared the SynBioNF-enabled SERS platform and commercially available LFA by testing several clinical samples with known Ct values (Supplementary Fig. 16), in which the former successfully detected all the positive samples, whereas the latter failed to find three positive samples. Similarly, both SynBioNF-enabled SERS platform

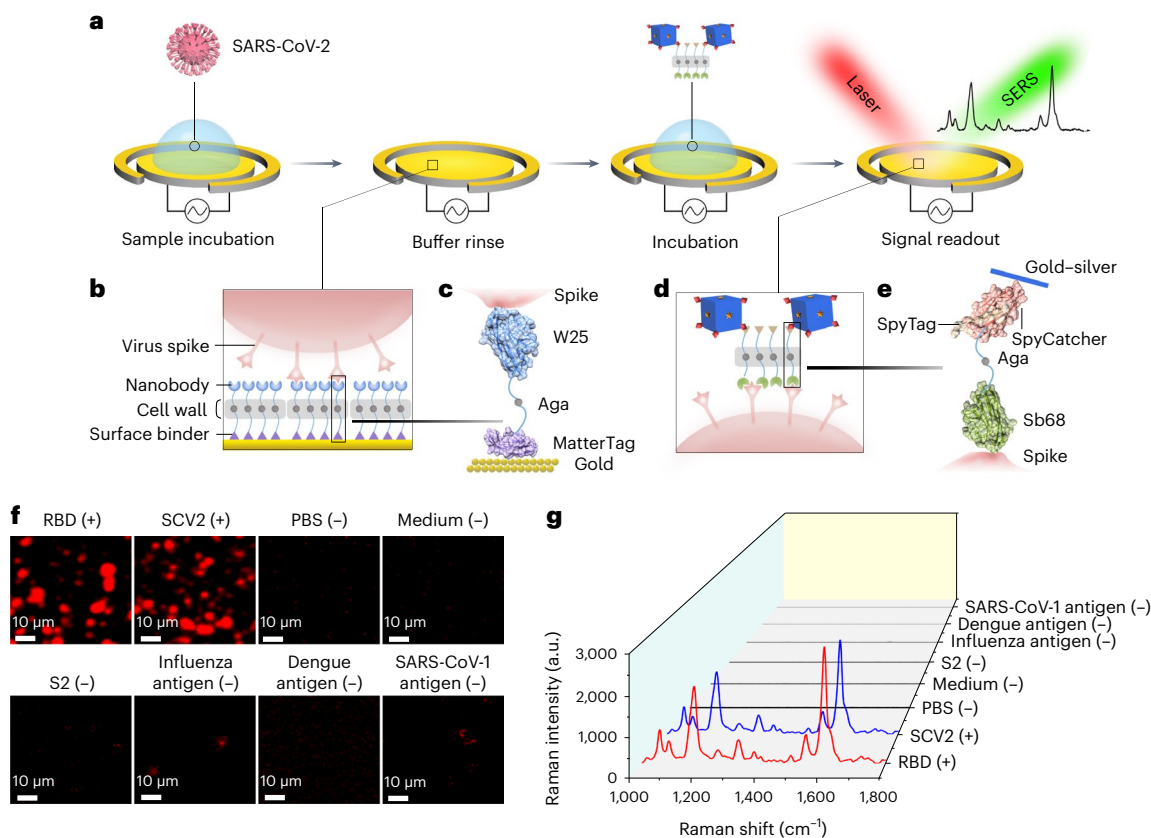


Fig. 5 | Schematic and specific detection of RBD and SCV2 by using SynBioNFs as capture and detection nanoprobes on the SERS platform. a, Schematic of the workflow of SCV2 detection. **b**, Immobilization of capturing SynBioNFs (W25–MatterTag) on the gold surface and the capture of virus from the sample. **c**, SynBioNFs using MatterTag to bind gold atoms and W25 nanobody to capture the RBD on the spike protein. **d**, Identification of the captured virus by detection SynBioNFs (Sb68–SpyTag) conjugated with nanoboxes. **e**, SynBioNFs using

SpyTag to conjugate SpyCatcher-coated gold–silver alloy surface and Sb68 nanobody to detect the RBD on the spike protein. **f,g**, SERS mapping images (**f**) and average Raman spectra (**g**) in the presence of positive samples and negative controls. The red colour in **f** indicates the presence of RBD/SCV2 on the gold microelectrodes, which clearly differentiated the positive samples from the negative controls.

and LFA did not generate very consistent signals with the Ct values in RT-qPCR based on the different working principles. Importantly, the SynBioNF-enabled SERS platform generated concentration-dependent results in the measurement of healthy samples spiked with different concentrations of SCV2 virions (Fig. 6g). The LFA also produced a similar concentration-dependent trend (Fig. 6h), but the detection failed on the use of SCV2 concentration lower than 2×10^4 virions ml^{-1} . Taken together, these comparisons illustrated the capability of SynBioNFs in the highly sensitive screening of COVID-19 patients.

SynBioNF-enabled SCV2 detection on other platforms

To further demonstrate the diverse utility of this nanoprobe for disease detection, we explored its application of SCV2 detection on three widely used platforms, including fluorescence, electrochemical and visual colorimetric LFA systems.

To enable a convenient fluorescence readout, we fused a StrepTag on SynBioNFs to conjugate with commercially available streptavidin fluorescent beads for detection. Specifically, following the capture of SCV2 by SynBioNFs (Sb68–MatterTag) on gold surfaces, SynBioNFs (Nb21–StrepTag) bioconjugated with fluorescent beads detected RBD through fluorescence imaging. As shown in Extended Data Fig. 1a, the presence of SCV2 generated clear fluorescence signals compared with the negligible signals from the medium control, which suggested the possibility of SynBioNFs on fluorescence diagnostic platforms.

For portable electrochemical sensors, SynBioNFs enabled a simple and rapid label-free DPV target detection. To illustrate this, SynBioNFs (Sb68–MatterTag) on disposable screen-printed electrodes were used to capture SCV2, which resulted in increased surface impedance and reduced peak current signals for quantification. In Extended Data Fig. 1b,c, the current decreased, and therefore, a higher percentage of peak current change was observed for SCV2 but not the medium control. The shifted and broadened DPV peak after SCV2 capture was probably triggered by the formation of a biomolecule layer that decreased the effective current density on the electrodes^{27–29}. The corresponding CV result further indicated the successful detection of SCV2 (Extended Data Fig. 1d) with the appearance of characteristic redox peaks.

For the LFA, SynBioNFs can be conjugated with gold nanoparticles to visually identify target binding through the specific colour. In this regard, we linked SynBioNFs (Nb21–SpyTag) and gold nanoparticles (coated with SpyCatcher) as bioconjugates through the SpyTag/SpyCatcher system. After capturing SCV2 on the paper-based analytical device, the bioconjugates can recognize the SCV2 RBD for red colour readout. The apparent red colour generated by SCV2 and no colour from the medium negative control (Extended Data Fig. 1e) in the test lines indicated the feasibility of SynBioNFs on LFA devices. Furthermore, SynBioNF-enabled LFA showed clear differences between one SCV2 Omicron sample and one healthy clinical sample (Supplementary Fig. 17).

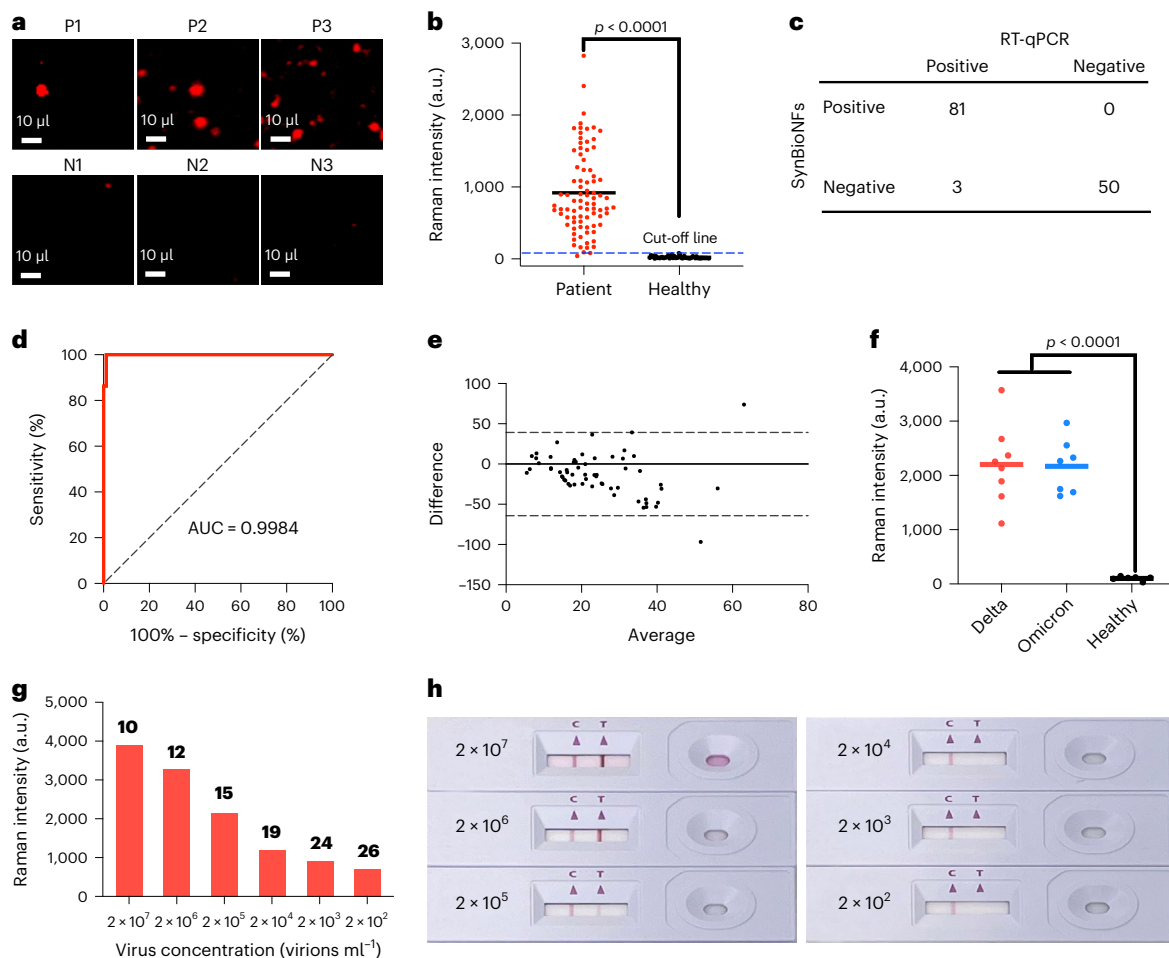


Fig. 6 | SynBioNF-enabled SERS screening of clinical samples for COVID-19 patient screening. **a**, Representative Raman images of identified three positive (P1–P3) and three negative (N1–N3) samples. The red colour indicates the presence of SCV2 on the gold microelectrodes, which clearly differentiates the positive samples from the negative controls. Data from three independent experiments. **b**, Raman intensities of all the clinical samples, with the horizontal lines showing the mean values ($n = 134$ biologically independent samples) ($p < 0.0001$, two-tailed t -test). **c**, Classification result of SynBioNF-based SCV2 detection with the use of the cut-off value (that is, 94) and correlation with RT-qPCR diagnosis. **d**, Receiver operating characteristic curve of patient versus

healthy detection. AUC, area under the curve. **e**, Bland–Altman plot of SynBioNF-enabled and RT-qPCR detection. **f**, Raman intensities for the detection of SCV2 Delta variant, Omicron variant and healthy clinical sample controls, with the horizontal lines showing the mean values ($n = 21$ biologically independent samples) ($p < 0.0001$, two-tailed t -test). **g, h**, Detection of healthy samples spiked with different concentrations of SCV2 virions showing Raman intensities with Ct values labelled on the top of the columns (**g**) and the corresponding commercially available LFA photographs (**h**), in which LFA failed to generate visible signals on the use of SCV2 concentration lower than 2×10^4 virions ml^{-1} .

Conclusions

SynBioNFs represent the next generation of nanoprobe, which are cost-effective and simple-to-manufacture reagents featuring many key advantages for biomarker detection compared with traditional probes on the market. These include (1) the genetically ‘plug and play’ programmable display of an array of potent nanobodies on nanosized yeast cell walls for potential high-avidity ‘molecular Velcro-like’ target binding; and (2) the integration of functional tags for simple, controlled and site-specific nanobody immobilization on flat or micro-/nanoparticle surfaces. These advantages enabled SynBioNFs as convenient nano-reagents to apply on different platforms for biomarker detection. We have demonstrated streamlined and effective nanoprobe functionalization on the surfaces of flat (that is, gold microelectrodes) and micro-/nanoparticles (that is, gold–silver alloy nanoboxes, fluorescent beads and spherical gold nanoparticles). All these properties of SynBioNFs synergistically benefit highly effective biomarker detection. More detailed discussions on the utility and advantages of SynBioNFs are provided in Supplementary Information.

Online content

Any methods, additional references, Nature Portfolio reporting summaries, source data, extended data, supplementary information, acknowledgements, peer review information; details of author contributions and competing interests; and statements of data and code availability are available at <https://doi.org/10.1038/s41565-023-01415-1>.

References

- Li, W. et al. Emerging nanotechnologies for liquid biopsy: the detection of circulating tumor cells and extracellular vesicles. *Adv. Mater.* **31**, 1805344 (2018).
- Li, J. et al. Amplification-free SARS-CoV-2 detection using nanoyeast-scFv and ultrasensitive plasmonic nanobox-integrated nanomixing microassay. *Anal. Chem.* **93**, 10251–10260 (2021).
- Mina, M. J., Parker, R. & Larremore, D. B. Rethinking COVID-19 test sensitivity—a strategy for containment. *N. Engl. J. Med.* **383**, e120 (2020).
- Ma, W. et al. Modular assembly of proteins on nanoparticles. *Nat. Commun.* **9**, 1489 (2018).

5. Dong, X.-H., Obermeyer, A. C. & Olsen, B. D. Three-dimensional ordered antibody arrays through self-assembly of antibody-polymer conjugates. *Angew. Chem. Int. Ed.* **56**, 1273–1277 (2017).
6. Xiang, Y. et al. Versatile and multivalent nanobodies efficiently neutralize SARS-CoV-2. *Science* **370**, 1479–1484 (2020).
7. Valenzuela Nieto, G. et al. Potent neutralization of clinical isolates of SARS-CoV-2 D614 and G614 variants by a monomeric, sub-nanomolar affinity nanobody. *Sci. Rep.* **11**, 3318 (2021).
8. Ahmad, J. et al. Structures of synthetic nanobody-SARS-CoV-2 receptor-binding domain complexes reveal distinct sites of interaction. *J. Biol. Chem.* **297**, 101202 (2021).
9. Guo, K. et al. Rapid single-molecule detection of COVID-19 and MERS antigens via nanobody-functionalized organic electrochemical transistors. *Nat. Biomed. Eng.* **5**, 666–677 (2021).
10. Yang, E. Y. & Shah, K. Nanobodies: next generation of cancer diagnostics and therapeutics. *Front. Oncol.* **10**, 1182 (2020).
11. Dedisch, S. et al. Matter-tag: a universal immobilization platform for enzymes on polymers, metals, and silicon-based materials. *Biotechnol. Bioeng.* **117**, 49–61 (2020).
12. Schmidt, T. G. M. & Skerra, A. The Strep-tag system for one-step purification and high-affinity detection or capturing of proteins. *Nat. Protoc.* **2**, 1528–1535 (2007).
13. Mancini, R. J., Lee, J. & Maynard, H. D. Trehalose glycopolymers for stabilization of protein conjugates to environmental stressors. *J. Am. Chem. Soc.* **134**, 8474–8479 (2012).
14. Farokhinejad, F. et al. Generation of nanoyeast single-chain variable fragments as high-avidity biomaterials for dengue virus detection. *ACS Biomater. Sci. Eng.* **7**, 5850–5860 (2021).
15. Walker, R. S. K. & Pretorius, I. S. Applications of yeast synthetic biology geared towards the production of biopharmaceuticals. *Genes* **9**, 340 (2018).
16. Chao, G. et al. Isolating and engineering human antibodies using yeast surface display. *Nat. Protoc.* **1**, 755–768 (2006).
17. Yang, X. et al. Development of novel surface display platforms for anchoring heterologous proteins in *Saccharomyces cerevisiae*. *Microb. Cell Fact.* **18**, 85 (2019).
18. Ferrara, F. et al. Using phage and yeast display to select hundreds of monoclonal antibodies: application to antigen 85, a tuberculosis biomarker. *PLoS ONE* **7**, e49535 (2012).
19. Teymennet-Ramírez, K. V., Martínez-Morales, F. & Trejo-Hernández, M. R. Yeast surface display system: strategies for improvement and biotechnological applications. *Front. Bioeng. Biotechnol.* **9**, 794742 (2021).
20. Li, J. et al. The growing impact of micro/nanomaterial-based systems in precision oncology: translating ‘multiomics’ technologies. *Adv. Funct. Mater.* **30**, 1909306 (2020).
21. Najjar, D. et al. A lab-on-a-chip for the concurrent electrochemical detection of SARS-CoV-2 RNA and anti-SARS-CoV-2 antibodies in saliva and plasma. *Nat. Biomed. Eng.* **6**, 968–978 (2022).
22. Fischer, L. M. et al. Gold cleaning methods for electrochemical detection applications. *Microelectron. Eng.* **86**, 1282–1285 (2009).
23. Goud, K. Y. et al. An electrochemical aptasensor based on functionalized graphene oxide assisted electrocatalytic signal amplification of methylene blue for aflatoxin B1 detection. *Electrochim. Acta* **244**, 96–103 (2017).
24. Koo, K. M., Dey, S. & Trau, M. Amplification-free multi-RNA-type profiling for cancer risk stratification via alternating current electrohydrodynamic nanomixing. *Small* **14**, 1704025 (2018).
25. Vogels, C. B. F. et al. Analytical sensitivity and efficiency comparisons of SARS-CoV-2 RT-qPCR primer-probe sets. *Nat. Microbiol.* **5**, 1299–1305 (2020).
26. Wyllie, A. L. et al. Saliva or nasopharyngeal swab specimens for detection of SARS-CoV-2. *N. Engl. J. Med.* **383**, 1283–1286 (2020).
27. Safarzadeh, M. et al. A label-free DNA-immunosensor based on aminated rGO electrode for the quantification of DNA methylation. *Nanomaterials* **11**, 985 (2021).
28. Moulton, S. E., Barisci, J. N., Bath, A., Stella, R. & Wallace, G. G. Investigation of protein adsorption and electrochemical behavior at a gold electrode. *J. Colloid Interface Sci.* **261**, 312–319 (2003).
29. Anzai, J.-I., Guo, B. & Osa, T. Electrochemically accelerated adsorption of serum albumin on the surface of platinum and gold electrodes. *Chem. Pharm. Bull.* **42**, 2391–2393 (1994).

Publisher’s note Springer Nature remains neutral with regard to jurisdictional claims in published maps and institutional affiliations.

Springer Nature or its licensor (e.g. a society or other partner) holds exclusive rights to this article under a publishing agreement with the author(s) or other rightsholder(s); author self-archiving of the accepted manuscript version of this article is solely governed by the terms of such publishing agreement and applicable law.

© The Author(s), under exclusive licence to Springer Nature Limited 2023

Methods

Chemicals and materials

Hydrogen tetrachloroaurate trihydrate, silver nitrate, dithiobis (succinimidyl propionate), 11-mercaptoundecanoic acid (MUA) and MMC were purchased from Sigma-Aldrich. Analytical-grade ascorbic acid was obtained from MP Biomedicals. 1-Ethyl-3-(3-dimethylaminopropyl) carbodiimide hydrochloride and *N*-hydroxysulfosuccinimide were obtained from Thermo Fisher Scientific. A Milli-Q water system was used to generate ultrapure water (18.2 MΩ cm) to synthesize the nanoparticles. Two commercially available LFA products purchased from Abbott (ARTG #345192) and SD Biosensor (ARTG #345219) were used to test the clinical samples by following the instructions from the providers.

Production of SpyCatcher, SpyTag and SCV2 RBD–mNeonGreen fusion proteins

To produce SpyCatcher and SpyTag, SpyCatcher–MatterTag and EGFP–SpyTag fusions were designed via a rigid linker (AEAAAKEAAK EAAAKA) and flexible linker (GGGS), respectively. The chimeric genes were commercially synthesized and cloned into the pCDNA3.1 vector. The fusion proteins were expressed in ExpiCHO-S cells according to the manufacturer's instructions (Thermo Fisher Scientific). For purification, the filtered supernatant was loaded on a Strep-Tactin 4Flow column (IBA Lifesciences) equilibrated with a purification buffer (100 mM Tris–HCl (pH 8.0), 150 mM NaCl). The column was then washed with 50 column volumes of purification buffer. The fusion protein was eluted by a purification buffer containing 50 mM biotin (IBA Lifesciences). The purities of the purified proteins were analysed in sodium dodecyl sulfate–polyacrylamide gel electrophoresis. The expression and purification of SCV2–mNeonGreen fusion protein is described elsewhere².

Engineering yeast cells and production of multifunctional SynBioNFs

EBY100 yeast cells were employed to display eight different functional fusion proteins on the cell walls, including (1) W25–MatterTag, (2) Sb68–SpyTag, (3) Sb68–MatterTag, (4) Nb21–StrepTag, (5) Nb21–SpyTag, (6) Nb21–MatterTag, (7) DD7–MatterTag and (8) DD5–SpyTag. These fusion gene sequences were commercially synthesized and cloned (Gene Universal; Supplementary Data 1 and 2) into the pCTCON2 expression plasmid for yeast surface display by following previous work². In our design, the target-binding nanobodies (Sb68, W25 and Nb21) and functional peptide tags (MatterTag, SpyTag and StrepTag) were fused into the N and C termini of Aga2p, respectively. A flexible linker (GGGS) with 15 and 30 amino acids was used at the N and C termini of Aga2p to avoid steric hindrances between the fused proteins/peptides. Furthermore, HA and c-Myc peptide tags that allow the quantification of the displayed fusion proteins were included at the N and C termini of each gene construct, respectively. The fusion proteins carrying Aga2p were able to immobilize on the yeast cell walls by interacting with the Aga1p anchor protein.

To achieve the fusion protein display, EBY100 yeast cells were incubated with recombinant DNA (10 µl, 1,000 ng) under the stimulation of a square wave using electroporation. The produced yeast cells were cultured in the SDCAA medium and monitored until the optical density at 600 nm (OD₆₀₀) reached 5–10. The yeast cells were then transferred into galactose containing the SGCAA medium and diluted to OD₆₀₀ of 1.0 to induce fusion protein expression. Following the culture for 48 h, the yeast cells were collected and confirmed the fusion protein expression by performing a flow cytometry analysis, as described below.

For the preparation of SynBioNFs, the yeast cells with the display of fusion proteins were collected from the SGCAA medium (50 ml, OD₆₀₀ of 6–10) and washed with PBS through centrifugation (2,000×g, 10 min), followed by resuspending into PBS supplemented with a protease

inhibitor cocktail with EDTA (10 ml per tablet). The mechanical fragmentation of yeast cells was conducted using a sonicator (Sonics ultrasonic processor VC-505) with a 3 mm tip diameter and 171 mm length at an ultrahigh intensity by repeating the following conditions for five times: 40% amplitude; 1 s ON and 1 s OFF pulse for 2 min. Ultimately, SynBioNFs were obtained using centrifugation (2,500×g, 15 min) to collect the supernatant products and purified through a filter unit (100 nm, Millipore).

Flow cytometry profiling of fusion proteins

The yeast cells with fusion protein expression (10⁷ cells ml⁻¹) were collected and washed using PBS containing 0.1% bovine serum albumin (BSA) (500 µl) through centrifugation (1,500×g, 4 min) at 4 °C. To enable the labelling of the yeast surface protein, the yeast cells were incubated with anti-Myc antibody labelled with DyLight 650 (1:100 dilution) and RBD–mNeonGreen, or anti-dengue NS1 protein followed by anti-His antibody labelled with PE (1:100 dilution) in PBS containing 0.1% BSA (100 µl) with rotation and away from light at 4 °C for 1 h. The labelled yeast cells were centrifuged (1,500×g, 4 min) and washed with PBS containing 0.1% BSA (500 µl), followed by resuspending them into PBS containing 0.1% BSA (500 µl) for testing. The yeast cell controls without the use of anti-Myc or anti-His, anti-dengue NS1 antibody and RBD–mNeonGreen were prepared with the same protocol. The obtained yeast cells were subject to flow cytometry profiling (CytOFLEX, Beckman Coulter) using two lasers (488 and 633 nm) and two band-pass filters (525/40 and 660/20 nm). The data were acquired using CytExpert (2.4.0.28) and analysed with FlowJo software (10.8.1).

SCV2 culturing using cell line

SCV2 was cultured in Vero E6 cells. The Vero E6 cells were first cultured in Dulbecco's modified Eagle's medium supplemented with 2% heat-inactivated foetal bovine serum. When the cells were 70–90% confluent, the viral inoculum was inoculated into the Vero E6 cells and incubated at 37 °C (5% CO₂); the cytopathic effect was observed. SCV2 was harvested in the supernatant via centrifugation at 4,500×g for 10 min. Virus was gamma irradiated at a dose of 50 kGy to inactivate it.

RT-qPCR quantification of cultured SCV2

To quantify the cultured SCV2 stock, RT-qPCR was performed. MagMAX-96 viral RNA isolation kit was used to extract the SCV2 RNA. The gBlock synthetic E gene standards were utilized to establish the copy-number-related calibration curve. The test employed the AgPath-ID One-Step RT-PCR master mix with the following primers: CoV-E-fwd (5'-AGT ACG AAC TTA TGT ACT CAT TCG TT-3'), CoV-E-R2 (5'-ATA TTG CAG CAG TAC GCA CAC A-3') and TaqMan probe (CoV E probe 5'-6-FAM-ACA CTA GCC ATC CTT ACT GCG CTT CG-MGB-3'). The detection of SCV2 was conducted in duplicates by using the mean for calibration on an Applied Biosystems instrument. The cycling conditions were 45 °C for 10 min and 95 °C for 10 min, followed by 45 cycles of 95 °C for 15 s and 60 °C for 45 s.

Conjugating detection SynBioNFs with gold–silver alloy nanoboxes

The conjugation of SynBioNFs with gold–silver alloy nanoboxes was performed via the SpyCatcher-/SpyTag-mediated self-assembly. SpyCatcher-coated gold–silver alloy nanoboxes were first prepared as follows: gold–silver alloy nanoboxes were synthesized following our previous work³⁰. One millilitre of nanoboxes were centrifuged at 800×g for 15 min. Then, 10 µl Raman reporter (MMC) and 2 µl linker molecule (MUA) were incubated with the above nanoboxes for 5 h. After removing the free MMC and MUA by centrifuging at 800×g for 15 min, 10 µl of 1-ethyl-3-(3-dimethylaminopropyl) carbodiimide hydrochloride (10 mM) and 20 µl of *N*-hydroxysulfosuccinimide (10 mM) were added to activate the carboxyl group on MUA. Then, 0.5 µg SpyCatcher was incubated with the nanoboxes for 30 min at room temperature.

The SpyCatcher-coated nanoboxes were purified with centrifuging at $800\times g$ for 15 min and resuspended into 200 μl of 0.1% BSA.

Next, 30 μl of the SpyCatcher-coated nanoboxes were incubated with 4 μl of SynBioNFs (Sb68–SpyTag) ($8\ \mu\text{g}\ \mu\text{l}^{-1}$) in 60 μl of 10 mM PBS, 1 mM BSA and 1% BSA buffer for 10 min. The final products were collected by centrifuging at $600\times g$ for 10 min and washing with 0.1% BSA.

NanoFCM characterization of SynBioNFs and nanobox bioconjugates

NanoFCM measurements were performed on a nanoFCM flow NanoAnalyser (NanoFCM). The NanoAnalyser was first calibrated for concentration and size using the standard nanoparticles provided by the company. The size distribution of SynBioNFs was obtained by comparing with the cocktail size standard (that is, premixed silica nanoparticles with different diameters). To profile the fluorescence profiling of gold–silver alloy-nanobox-conjugated SynBioNFs against RBD–mNeonGreen, 30.0 μl of the conjugates were incubated with 0.5 μl of RBD–mNeonGreen (350 μM) at room temperature for 30 min and the products were washed three times with 0.1% BSA via centrifugation at $600\times g$ for 10 min, followed by recording the events for 1 min. The same amount of gold–silver alloy nanobox and SynBioNFs without reacting with RBD–mNeonGreen were used as negative controls to set the threshold.

SynBioNF-enabled SERS detection of RBD, SCV2, simulated patient samples and clinical COVID-19 samples

The gold microelectrodes were prepared in-house by a photolithography approach with 4-inch borosilicate glass wafers and following a previously established protocol³¹. After photolithography, the wafer consisted of an array of 28 circular gold microelectrodes with inner working electrodes (1.00 mm in diameter) and outer counter electrode (0.12 mm in diameter). The working and counter electrodes were separated by 1 mm. To contain the sample on the gold microelectrodes, a well structure made of polydimethylsiloxane was attached to the wafer. Before functionalization, the gold microelectrodes were washed with $1\times$ PBS. Subsequently, SynBioNFs (Sb68–MatterTag) were pipetted on the gold microelectrodes and incubated for 30 min at room temperature. Excess SynBioNFs (Sb68–MatterTag) were removed by washing three times with $1\times$ PBS. Finally, the gold microelectrodes were blocked with 5% BSA in $1\times$ PBS for 1 h at room temperature. Before use, the gold microelectrodes were washed with $1\times$ PBS. A 30 μl mixture of the patient sample (20 μl sample + 10 μl PBS/1% Tween-80) was then pipetted on the gold microelectrode and incubated for 45 min under stimulation of nanomixing by alternating-current electrohydrodynamics (frequency, 500 Hz; amplitude, 800 mV). In particular, the inclusion of PBS/1% Tween-80 buffer in the patient samples was aimed to inactivate the virus. For clinical samples that are not contagious after treatment (for example, gamma irradiation), the samples can be directly applied on the platform without the use of PBS/1% Tween-80 buffer. Subsequently, after washing the gold microelectrodes with $1\times$ PBS, the bioconjugates of SynBioNFs (Sb68–MatterTag) and nanoboxes were incubated for 20 min under the same nanomixing conditions as above. Finally, the excess bioconjugates were removed by washing with $1\times$ PBS. The gold microelectrodes were then subject to confocal Raman mapping (WITec alpha300 R spectrometer) and collecting/analysing the data using WITec Suite FIVE software. Specifically, a He–Ne laser with an excitation wavelength of 632.8 nm, $\times 20$ objective, electron-multiplying charge-coupled device camera, 0.05 s integration time and 1 μm step size was used for scanning the images with a size of 60 $\mu\text{m} \times 60\ \mu\text{m}$.

Clinical sample details

SCV2-positive clinical patient samples were supplied by the Molecular Diagnostics Unit at Pathology Queensland, and consisted of nasopharyngeal swabs resuspended in PBS. These samples were tested

using in vitro diagnostics RT-qPCR at the Molecular Diagnostics Unit very early in the pandemic, whereas diagnostic assays were still being completely validated. Negative and positive samples were provided by the Infectious Diseases Laboratory, Microbiology Prevention Division, Pathology Queensland, and tested using the validated BGI platform. Patient samples were collected under the following ethics approval: HREC ref. no. HREC/2020/QRBW/70461; project title, optimizing clinical diagnostics for SCV2. A waiver of consent was approved by this ethics committee and compensation was not applicable for this study.

Fluorescent platform detection of SCV2

Sixty microlitres of SynBioNFs (Sb68–MatterTag) were incubated on the gold surface at room temperature for 2 h, followed by washing three times with PBS to remove free SynBioNFs. Then, 60 μl of the sample solution (that is, SCV2 or medium control) was loaded and incubated on the sensing area at room temperature for 1 h. The gold chips were washed with PBS three times to remove the uncaptured targets. Next, 50 μl of the bioconjugates were applied on the chips and incubated for 1 h. To prepare the bioconjugates, 500 μl SynBioNFs (Nb21–StrepTag) and 10 μl fluorescence beads (coated with streptavidin) were incubated in an Eppendorf tube at room temperature for 1 h and purified through centrifugation. After getting rid of the free bioconjugates, the gold chips were imaged under a fluorescence microscope. The acquired images were then analysed with ImageJ software (1.53).

Electrochemical detection of SCV2

Sixty microlitres of SynBioNFs (Sb68–MatterTag) were incubated on the screen-printed electrodes at room temperature for 2 h. After washing away the free SynBioNFs (Sb68–MatterTag), 60 μl of the sample solution (that is, SCV2 or medium control) was applied on the inner circular working electrodes for an incubation of 1 h and subsequently washed three times with PBS for electrochemical detection. For DPV measurement, 40 μl of 2.5 mM $[\text{Fe}(\text{CN})_6]^{3-}/[\text{Fe}(\text{CN})_6]^{4-}$ redox couple in $1\times$ PBS (pH 7.4) containing 0.1 M KCl was added onto the screen-printed electrodes to record the current. The DPV scan was conducted on an electrochemical analyser CHI 650D (CH Instruments) using a scan voltage from -0.2 to 0.4 V, pulse amplitude of 50 mV, pulse width of 50 ms, potential step of 5 mV and pulse period of 10 ms. The CV measurements were performed in 10 mM PBS in the presence of the $[\text{Fe}(\text{CN})_6]^{3-}/^{4-}$ redox system (pH 7.4, 2.5 mM $[\text{Fe}(\text{CN})_6]^{3-}/^{4-}$). The data were recorded between -0.6 and 0.6 V at a scan rate of $100\ \text{mV}\ \text{s}^{-1}$.

LFA for SCV2 detection

Lateral flow test strips (width, 7 mm; length, 80 mm) were prepared using nitrocellulose HP-80 FF strips with laminate backing (Cytiva) and medium-sized absorbent pads attached at the top of the strips. Multiple strips were prepared using a programmable high-speed strip cutter (KinBio). Each strip was spotted with 0.2 μl (200 ng) of capture CR3022 monoclonal antibodies and dried in a $37\ ^\circ\text{C}$ incubator for 15 min. The CR3022 antibodies were prepared in-house using Chinese hamster ovary cell culture.

Samples for the lateral flow strips were set up in 0.2 ml thin-walled tubes and incubated at $37\ ^\circ\text{C}$ for 10 min. Next, 10 μl of bioconjugates of SynBioNFs (Nb21–SpyTag) and spherical gold nanoparticles (coated with SpyCatcher) in PBS was mixed with 10 μl SCV2 or medium control. Then, 1% BSA and 1% Tween-80 were included in each reaction. Each reaction was incubated at $37\ ^\circ\text{C}$ for 15 min. The whole reaction (20 μl) was aliquoted into wells of a 96-well plate, and the test strips were dipped into the wells to allow the samples to run vertically up the strips towards the absorbent pad for 1–2 min. Then, 50 μl PBST ($1\times$ PBS + 0.05% Tween-20) was added to the wells and incubated for further 5 min to move all the bioconjugates up the strip. Visual colorimetric reactions at the capture line were imaged using a digital camera.

ELISA-based assay for stability and avidity test

For the ELISA assay, $10 \mu\text{g ml}^{-1}$ of recombinant SCV2 RBD protein diluted in $1\times$ TBS (20 mM Tris (pH 8.0), 300 mM NaCl) was coated on MaxiSorp ELISA plate wells for 1 h at room temperature. The wells were then incubated with the blocking buffer (3.00% BSA in TBS with 0.05% Tween-20) for 1 h at room temperature. Then, 100 μl of anti-SCV2 RBD SynBioNFs (Nb21–SpyTag) (1:5) or rabbit polyclonal antibody (1:10,000) were added to each well and incubated for 1 h at room temperature. For a thermal stability analysis, SynBioNFs or rabbit polyclonal antibody aliquots were incubated at the indicated temperature for 1 h and subsequently added into the respective wells. For avidity assay, urea, guanidine hydrochloride, Triton X-100, sodium dodecyl sulfate or NaCl were added at the indicated concentrations for 1 h at room temperature. To test the acidic pH conditions, a mix of citric acid and sodium phosphate buffers (pH, 2.6–7.6) were used. For alkaline pH conditions, a mix of sodium carbonate and sodium bicarbonate buffers (pH, 9.2–10.8) were used. After washing the wells with TBST five times, HRP-conjugated anti-Myc tag antibody (1:5,000 dilution in 3% BSA–TBST) or HRP-conjugated goat anti-rabbit IgG secondary antibody (1:10,000) was added to the wells for 1 h. The wells were washed with TBST and finally 100 μl of TMB substrate was added to each well, and the reaction was stopped by 100 μl of 1 M sulfuric acid.

Octet assay for measurement of protein interaction

Streptavidin sensors (ForteBio) were pretreated in 200 μl of 10 mM PBS for 10 min. Each well was loaded with 200 μl of the solution. The assay was performed by setting a program: the sensors were dipped in PBS for 120 s in the initial baseline step, loaded with 75 μg of strep RBD per well in the loading sample, dipped in PBS for 120 s in the second baseline step, interacted with SynBioNFs (Nb21–SpyTag) or soluble Nb21 nanobody for 300 s in the association step and ended with dissociation in PBS for 600 s.

Statistical analysis

The diagnostic sensitivity, specificity and accuracy of the SynBioNF-based screening of clinical samples on the SERS platform were determined based on the confusion matrix (Fig. 6c) with the following formulas:

Sensitivity = Number of true positive assessments / Number of all positive assessments = $81/(81 + 3) = 96.43\%$;

Specificity = Number of true negative assessments / Number of all negative assessments = $50/(0 + 50) = 100\%$;

Accuracy = Number of correct assessments / Number of all assessments = $(81 + 50)/(81 + 3 + 0 + 50) = 97.76\%$.

Two-tailed *t*-tests, receiver operating characteristic curve and Bland–Altman analysis were performed in GraphPad Prism (v. 9.2).

Reporting summary

Further information on research design is available in the Nature Portfolio Reporting Summary linked to this article.

Data availability

The data that support the findings of this study are available within the paper and its Supplementary Information. Source data are provided with this paper.

References

- Li, J. et al. A digital single-molecule nanopillar SERS platform for predicting and monitoring immune toxicities in immunotherapy. *Nat. Commun.* **12**, 1087 (2021).
- Wang, J. et al. Characterizing the heterogeneity of small extracellular vesicle populations in multiple cancer types via an ultrasensitive chip. *ACS Sens.* **6**, 3182–3194 (2021).

Acknowledgements

We acknowledge funding from the ARC DPs (160102836, 140104006, 210103151 and 220100960) that stimulated the current research. We would like to thank the Infectious Diseases Laboratory, Pathology Queensland, Brisbane, Australia (particularly, A. Bordin), for the clinical specimens used in this study. J.L. and S.E. acknowledge support from the Commonwealth Scientific and Industrial Research Organisation. A.W. thanks the National Health and Medical Research Council of Australia for funding (APP1173669). C.B.H. acknowledges funding support from the Advance Queensland Industry Research Fellowship—COVID 19 (AQIRF104-2020-CV). We acknowledge the facilities, and the scientific and technical assistance, of the Australian Microscopy & Microanalysis Research Facilities at the Centre for Microscopy and Microanalysis, The University of Queensland. We also thank the technical and scientific guidance from the Queensland node of the Australian National Fabrication Facility (ANFF-Q) in confocal Raman mapping and gold microelectrode fabrication.

Author contributions

J.L. conceptualized the project, designed and executed bioconjugation and SERS experiments, analysed the data, prepared the figures and contributed to writing the manuscript. C.B.H. designed, executed and analysed the lateral flow experiments; guided the experimental design, data analysis and clinical sample testing; and contributed to manuscript writing. S.D. designed, executed and analysed the experiments associated with the electrochemical- and fluorescence-based platforms. K.L. and D.M.W. provided the patient samples and lab facilities for clinical sample testing; K.L. also performed the experiments and analysed the data. S.P. and S.R. designed and guided the project process. R.J.L. helped in the design, execution and data analysis of the nanoflow cytometry experiments. A.W. guided the experimental design, data analysis and executed the SERS experiments and contributed to manuscript preparation. S.E. conceptualized the project, designed the SynBioNFs concepts and constructs, executed the experiments, analysed the data, prepared the figures and contributed to writing the manuscript. M.T. conceptualized and supervised the progression of the project and guided the experimental design, data analysis and manuscript writing. All authors contributed to the preparation of the final manuscript.

Competing interests

The authors declare no competing interests.

Additional information

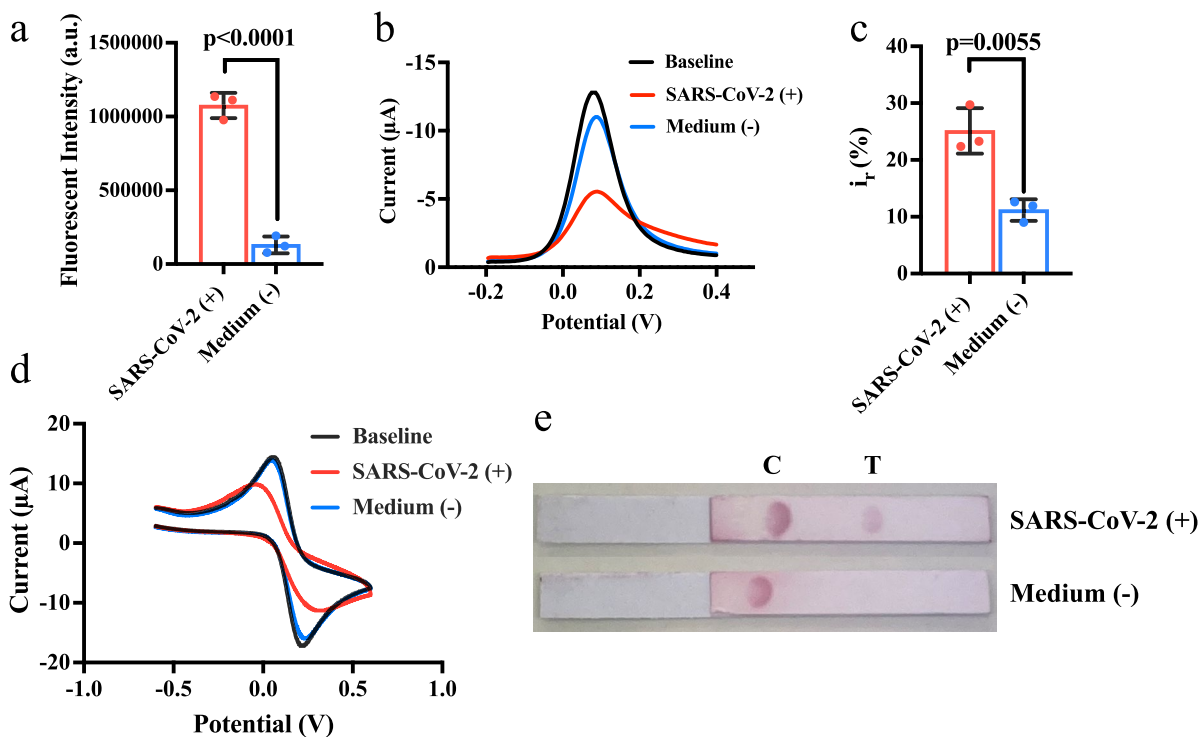
Extended data is available for this paper at <https://doi.org/10.1038/s41565-023-01415-1>.

Supplementary information The online version contains supplementary material available at <https://doi.org/10.1038/s41565-023-01415-1>.

Correspondence and requests for materials should be addressed to Christopher B. Howard, Alain Wuethrich, Selvakumar Edwardraja or Matt Trau.

Peer review information *Nature Nanotechnology* thanks the anonymous reviewers for their contribution to the peer review of this work.

Reprints and permissions information is available at www.nature.com/reprints.



Extended Data Fig. 1 | Demonstration of the utility of SynBioNFs to detect SCV2 on fluorescent, electrochemical, and naked eye platforms.

(a) Fluorescent platform showing different fluorescent intensities in the presence of SCV2 and medium control ($p < 0.0001$, two-tailed t test). Electrochemical measurement on SPEs showing (b) DPV graph, (c) percentage current change (that is, $[(i_{\text{Baseline}} - i_{\text{Target}})/i_{\text{Baseline}}] \times 100$) for SCV2 and medium control ($p = 0.0055$,

two-tailed t test), and (d) CV characterisation. Baseline refers to the DPV response of SPEs reacted with SynBioNFs (W25-MatterTag). (e) Naked eye based LFA testing SCV2 and medium control, in which C, T indicated control and test line, respectively. The control line was coated with SCV2 RBD. Data are presented as the mean values \pm standard deviation from three independent experiments.

Reporting Summary

Nature Portfolio wishes to improve the reproducibility of the work that we publish. This form provides structure for consistency and transparency in reporting. For further information on Nature Portfolio policies, see our [Editorial Policies](#) and the [Editorial Policy Checklist](#).

Statistics

For all statistical analyses, confirm that the following items are present in the figure legend, table legend, main text, or Methods section.

- | n/a | Confirmed |
|-------------------------------------|--|
| <input type="checkbox"/> | <input checked="" type="checkbox"/> The exact sample size (n) for each experimental group/condition, given as a discrete number and unit of measurement |
| <input type="checkbox"/> | <input checked="" type="checkbox"/> A statement on whether measurements were taken from distinct samples or whether the same sample was measured repeatedly |
| <input type="checkbox"/> | <input checked="" type="checkbox"/> The statistical test(s) used AND whether they are one- or two-sided
<i>Only common tests should be described solely by name; describe more complex techniques in the Methods section.</i> |
| <input checked="" type="checkbox"/> | <input type="checkbox"/> A description of all covariates tested |
| <input checked="" type="checkbox"/> | <input type="checkbox"/> A description of any assumptions or corrections, such as tests of normality and adjustment for multiple comparisons |
| <input type="checkbox"/> | <input checked="" type="checkbox"/> A full description of the statistical parameters including central tendency (e.g. means) or other basic estimates (e.g. regression coefficient) AND variation (e.g. standard deviation) or associated estimates of uncertainty (e.g. confidence intervals) |
| <input type="checkbox"/> | <input checked="" type="checkbox"/> For null hypothesis testing, the test statistic (e.g. F , t , r) with confidence intervals, effect sizes, degrees of freedom and P value noted
<i>Give P values as exact values whenever suitable.</i> |
| <input checked="" type="checkbox"/> | <input type="checkbox"/> For Bayesian analysis, information on the choice of priors and Markov chain Monte Carlo settings |
| <input checked="" type="checkbox"/> | <input type="checkbox"/> For hierarchical and complex designs, identification of the appropriate level for tests and full reporting of outcomes |
| <input checked="" type="checkbox"/> | <input type="checkbox"/> Estimates of effect sizes (e.g. Cohen's d , Pearson's r), indicating how they were calculated |

Our web collection on [statistics for biologists](#) contains articles on many of the points above.

Software and code

Policy information about [availability of computer code](#)

Data collection The flow cytometry data were acquired using CytExpert (2.4.0.28). SERS data were collected through WITec Suite FIVE software. ELISA data were collected using Tecan (Infinite 200 pro). SEM image was taken on JEOL-7100 FE-SEM microscope. Nanoflow cytometry was performed using Flow NanoAnalyzer.

Data analysis Flow cytometry data were analysed using FlowJo software (10.8.1). SERS images and spectra were analysed using WITec Suite FIVE software (5.0). Acquired fluorescent images were analysed with ImageJ software (1.53). Statistical analysis were performed using GraphPad (9.2).

For manuscripts utilizing custom algorithms or software that are central to the research but not yet described in published literature, software must be made available to editors and reviewers. We strongly encourage code deposition in a community repository (e.g. GitHub). See the Nature Portfolio [guidelines for submitting code & software](#) for further information.

Data

Policy information about [availability of data](#)

All manuscripts must include a [data availability statement](#). This statement should provide the following information, where applicable:

- Accession codes, unique identifiers, or web links for publicly available datasets
- A description of any restrictions on data availability
- For clinical datasets or third party data, please ensure that the statement adheres to our [policy](#)

The data that support the findings of this study are available within the paper and Supplementary Information. Source data are provided with this paper.

Human research participants

Policy information about [studies involving human research participants and Sex and Gender in Research](#).

Reporting on sex and gender	<p>These patients had the following sex and gender characteristics:</p> <p>0-9: 2 female and 4 male; 10-19: 3 female and 3 male; 20-29: 21 female and 9 male; 30-39: 7female and 25 male; 40-49: 9 female and 9male; 50-59: 11 female and 8 male; 60-69: 11 female and 12 male; 70-79: 7 female and 3 male; 11 patients have not stated or unknown age and sex</p>
Population characteristics	<p>Patient samples were not chosen by simple descriptive epidemiological markers, but rather by batches of remnant samples destined for disposal on the day of sample request from study co-authors. Participants were from the very early in the pandemic with the sex and gender characteristics listed above.</p>
Recruitment	<p>Self-selection bias was mitigated by the inclusion of subsequent Variants of Concern (VOC) in the sample population tested. Three dominant strains of SARS-CoV-2 were tested using this platform, thereby reducing the possible bias due to a single strain only. No potential self-selection bias or other biases were identified to impact the results.</p>
Ethics oversight	<p>Patient samples were collected under the following ethics approval. HREC reference number: HREC/2020/QRBW/70461. Project title: Optimising clinical diagnostics for SCV2. Specimen populations in this study consisted of respiratory samples submitted to a Queensland Pathology for diagnostic respiratory pathogen testing from 1/1/2020 to 31/12/2022 and had been marked for disposal. No participants were recruited to this study, therefore compensation was not applicable. In our ethics approval, our requirement for consent was waived by our ethical review body (https://www.nhmrc.gov.au/about-us/publications/national-statement-ethical-conduct-human-research-2007-updated-2018#toc__159). A waiver of consent was approved because: 1) involvement in the research carried no more than low risk to participants, 2) the benefits from the research justified any risks of harm associated with not seeing consent, 3) it was impractical to obtain consent (for example, due to the quantity, age or accessibility of records), 4) there was no known or likely reason for thinking that participants would not have consented if they had been asked, 5) there was sufficient protection of their privacy, 6) there was an adequate plan to protect the confidentiality of data, 7) in case the results had significance for the participants' welfare there was, where practicable, a plan for making information arising from the research available to them, 8) the possibility of commercial exploitation of derivatives of the data or tissue would not deprive the participants of any financial benefits to which they would be entitled, 9) the waiver was not prohibited by State, Federal, or international law.</p>

Note that full information on the approval of the study protocol must also be provided in the manuscript.

Field-specific reporting

Please select the one below that is the best fit for your research. If you are not sure, read the appropriate sections before making your selection.

Life sciences Behavioural & social sciences Ecological, evolutionary & environmental sciences

For a reference copy of the document with all sections, see [nature.com/documents/nr-reporting-summary-flat.pdf](https://www.nature.com/documents/nr-reporting-summary-flat.pdf)

Life sciences study design

All studies must disclose on these points even when the disclosure is negative.

Sample size	<p>Spare remnant patient samples were not readily available in Australia in 2021 and early 2022 at the time this study was conducted, therefore, sample sizes were dictated by the availability of samples kindly provided by Pathology Queensland. Samples were provided in batches upon request, if there was sufficient remnant material remaining after other testing was performed including next generation sequencing for contact tracing and public policy requirements.</p>
Data exclusions	<p>No data were excluded.</p>
Replication	<p>The experiments were performed in two to three independent replicates as properly indicated in the figure displays or figure legends. The replications had similar and consistent results in our research.</p>
Randomization	<p>Samples were randomly allocated.</p>
Blinding	<p>The experiments were blinded to the operator.</p>

Reporting for specific materials, systems and methods

We require information from authors about some types of materials, experimental systems and methods used in many studies. Here, indicate whether each material, system or method listed is relevant to your study. If you are not sure if a list item applies to your research, read the appropriate section before selecting a response.

Materials & experimental systems

- n/a Involved in the study
- Antibodies
- Eukaryotic cell lines
- Palaeontology and archaeology
- Animals and other organisms
- Clinical data
- Dual use research of concern

Methods

- n/a Involved in the study
- ChIP-seq
- Flow cytometry
- MRI-based neuroimaging

Antibodies

Antibodies used

Anti-Myc antibody was purchased from Abcam (ab117487).
 Anti-CR3022 antibody was prepared in house using CHO cell culture.
 Anti-RBD-mNeonGreen was prepared in house with ExpiCHO-S cells.
 Rabbit polyclonal antibody was bought from SinoBiological (40592-T62)
 PE conjugated anti-His antibody was purchased from Miltenyi Biotec(130-120-718)
 HRP conjugated anti-Myc tag antibody was obtained from Abcam (ab1326)
 HRP conjugated goat anti-rabbit IgG secondary antibody Invitrogen ThermoFisher Scientific (31460)

Validation

Anti-Myc antibody was validated by the manufacturer for immunocytochemistry, immunofluorescence, and flow cytometry use.
 CR3022 antibody was validated using ELISA and western blot.
 Anti-RBD-mNeonGreen was validated using SDS-PAGE and western blot.
 Rabbit polyclonal antibody was validated for ELISA and western blot use.
 Anti-His antibody was validated by the manufacturer for flow cytometry and intracellular flow cytometry use.
 HRP conjugated anti-Myc tag antibody was validated by the manufacturer for ELISA, western blot, and ICC use.
 HRP conjugated goat anti-rabbit IgG secondary antibody was validated by the manufacturer for western blot, IHC and IP applications.

Eukaryotic cell lines

Policy information about [cell lines and Sex and Gender in Research](#)

Cell line source(s)

Vero-E6 cell line was purchased from ATCC. CHO cell line and ExpiCHO-S cell lines were purchased from purchased from Thermo Fisher Scientific.

Authentication

The cell lines were directly used as received and none of the cell lines used were authenticated by ourselves.

Mycoplasma contamination

We run mycoplasma test to ensure the cells were free from mycoplasma contamination.

Commonly misidentified lines (See [ICLAC](#) register)

No misidentified cell lines were used in this study.

Flow Cytometry

Plots

Confirm that:

- The axis labels state the marker and fluorochrome used (e.g. CD4-FITC).
- The axis scales are clearly visible. Include numbers along axes only for bottom left plot of group (a 'group' is an analysis of identical markers).
- All plots are contour plots with outliers or pseudocolor plots.
- A numerical value for number of cells or percentage (with statistics) is provided.

Methodology

Sample preparation

The yeast cells with fusion protein expression (107 cells/mL) were collected and washed using PBS containing 0.1% BSA (500 μ L) through centrifugation (1500 g \times 4min) at 4 $^{\circ}$ C. To enable the labelling of yeast surface protein, the yeast cells were incubated with anti-Myc antibody labelled with DyLight650 (1:100 dilution) and RBD-mNeonGreen; or anti-Dengue-NS1 antibody followed by anti-His antibody labelled with PE (1:100 dilution) in PBS containing 0.1% BSA (100 μ L) with rotation and

	away from light at 4 °C for 1 h. The labelled yeast cells were centrifuged (1500 g × 4 min) and washed with PBS containing 0.1% BSA (500 µL), followed by resuspending them into PBS containing 0.1% BSA (500 µL) for testing. The yeast cell controls without the use of anti-Myc or anti-His, anti-Dengue-NS1 antibody, and RBD-mNeonGreen were prepared with the same protocol.
Instrument	Flow cytometry analysis was performed by using CytoFLEX Platform (Beckman Coulter) equipped with 488 and 633 nm lasers and 525/40 and 660/20 nm band-pass filters.
Software	Data were acquired in CyExpert and analysed in FlowJo software.
Cell population abundance	10,000 cells were recorded from each samples for analysis.
Gating strategy	The uninduced EBY100 yeast cells were used as control samples to set the gating levels.

Tick this box to confirm that a figure exemplifying the gating strategy is provided in the Supplementary Information.